Sensors & Actuators: B. Chemical 273 (2018) 211–219

Contents lists available at ScienceDirect

Sensors and Actuators B: Chemical

journal homepage: www.elsevier.com/locate/snb

A self-calibrated 2D nanoarchitecture for label-free SERS quantitation and distribution imaging of target

Jingxing Guo[1], Yunlong Chen[1], Jianqi Li, Jintong Liu, Huangxian Ju*

State Key Laboratory of Analytical Chemistry for Life Science, School of Chemistry and Chemical Engineering, Nanjing University, Nanjing 210023, PR China

ARTICLE INFO

Keywords:
Surface-enhanced Raman spectroscopy (SERS)
2D nanoarchitecture
Internal standard
SERS quantitation
Distribution imaging
Self-calibration

ABSTRACT

To achieve handy and reliable quantitative measurements of surface-enhanced Raman spectroscopy (SERS) for universal analysis, this work designs a self-calibrated 2D nanoarchitecture as a flexible sensor. This sensor consists of a self-assembled gold nanostars (AuNSs) monolayer sandwiched between two pieces of graphene, and can be easily attached on the surface of arbitrary samples. The inner AuNSs can offer a huge number of hot spots for strong Raman enhancement, and the existence of graphene further improves the stability and reproducibility of SERS signals for precise detection. By implanting Raman reporters as internal standard (IS) onto one side of the device and attaching the device with opposite side on sample surface, the distinct SERS signals from both IS and target can be quickly collected, which offers reliable quantification information of the target by IS calibration and has been demonstrated at the theoretical and experimental levels. Using carcinogenic dyestuff and agricultural fungicide as target models, this flexible nanoarchitecture realizes fast quantitative response to target in sample solution, and rapid in situ imaging of target distribution on solid surface. This sensor shows excellent reusability, good durability, and diversified structure collocation along with the simple operability, indicating great promise for fast on-site SERS detection in quantification and imaging applications.

1. Introduction

Nowadays, surface-enhanced Raman spectroscopy (SERS), which can provide fingerprint information of target molecules and allow ultrasensitive analysis down to the single-molecule level [1], has become a highly attractive analytical technology for various applications [2,3]. The dominant contribution of SERS comes from the greatly enhanced local electromagnetic fields (hot spots) in highly curved or gapped regions on SERS substrates. However, several challenges hinder the applications of SERS in quantitative analysis: (1) the enhancement is highly sensitive to the local nanostructure or surrounding environment [4], which makes it suffer from poor reproducibility and stability; (2) the main contribution of SERS signal usually originates from a small amount of target molecules inside surface hot spots, which leads to the heterogeneity of SERS substrate; (3) complex chemical interactions between target molecule and substrate may bring down the comparability between parallel SERS experiments [5]. Thus, the development of high-quality SERS substrates for efficient quantitative analysis is an urgent demand.

Improving the quantitative ability of SERS substrates can generally be achieved by two ways: artificially manipulating hot spots to obtain reproducible signals, or introducing internal standard (IS) to SERS systems. The former has been performed by constructing SERS substrates with uniform metal nanostructure arrays [6–9] or regulating nanogap distance [10,11], which unfortunately leads to harsh demands on equipment and operations, while the latter is relatively simple and can correct the environmental and matrix effects [12]. However, the competition of IS with the target molecules in sample solution to the surface adsorption sites of SERS substrates impairs the analytical performance. An efficient strategy to avoid the competitive adsorption has recently be developed by loading IS molecules on SERS-active nanoparticles, like core–shell nanoparticles [4,13,14], nanocapsules [15] and isolated-Au-nanocrystal [16]. The SERS measurements are then realized via chemically or physically aggregating the nanoparticles in the presence of target molecules [17], which confers scarce reproducibility and severe point-to-point variability [18] due to the difficulty to precisely control the colloidal aggregation for producing regular hot spots. Furthermore, the dynamic nature of the aggregated colloids also brings time-consuming problem to real sample testing. Thus, this technology is still far from becoming a convenient and reliable analytical tool for real applications.

Graphene has been demonstrated to enhance Raman signals due to

* Corresponding author.
E-mail address: hxju@nju.edu.cn (H. Ju).
[1] These authors contributed equally to this work.

https://doi.org/10.1016/j.snb.2018.06.029
Received 3 February 2018; Received in revised form 2 June 2018; Accepted 6 June 2018
Available online 12 June 2018
0925-4005/

its effective charge-transfer with adsorbed molecules, which is called as graphene-enhanced Raman scattering (GERS) effect [19–21]. Therefore, a graphene-mediated SERS substrate has been structured by depositing SERS-active metal nanoislands on graphene layer, which results in an atomically flat hot surface for Raman enhancement [5]. The combination of graphene with metallic nanostructures brings cleaner and more reproducible signals to other SERS substrates without obviously affecting their enhancement ability [22,23]. Therefore, graphene, as an emerging 2D nanomaterials, has gained more and more attention in SERS studies. In order to construct a high-quality SERS substrate for handy quantitative analysis, this work used graphene to design a self-calibrated 2D nanoarchitecture. This freestanding nanoarchitecture consisted of a self-assembled gold nanostars (AuNSs) monolayer sandwiched between two pieces of chemical vapor deposition (CVD)-grown monolayer graphene (1LG) as a graphene-AuNSs-graphene device (GAGD). The double-faced structure of GAGD could load IS and target molecules on different sides, which avoided the competition to the surface adsorption sites between IS and target. In addition, the dense AuNS monolayer offered a huge number of hot spots for producing highly sensitive SERS signals, and the presence of graphene not only separated the nanoparticles from the external environment but also evenly dispersed the target and IS on its surface, leading to more stable and reproducible SERS results. Thus, the flexible GAGD showed excellent stability, reusability and signal reproducibility, which are still important challenges in SERS testing systems. More importantly, through the IS calibration, GAGD could be used as an adhesive device to directly attach on the surface of arbitrary samples for fast quantitative monitoring of target concentration in solution and in situ SERS imaging of target distribution on solid surface. The strong interaction of graphene with different types of molecules, the modular design and easy preparation of the nanoarchitecture, and the simple operability assure the diversified structure collocation and the feasibility of this strategy as a universal protocol for SERS analysis.

2. Experimental

2.1. Materials and reagents

1LG prepared on Cu foil by CVD (1LG Cu foil) was purchased from ACS Materials (USA). Poly(methyl methacrylate) (PMMA, 2% wt in ethyl lactate) solution was obtained from Alresist (Germany). Chloroauric acid ($HAuCl_4 \cdot 3H_2O$), polyvinylpyrrolidone (PVP, MW = 10,000), sodium N-(2-hydroxyethyl) piperazine-N'-(2-ethanesulfonate) (HEPES), 1-dodecanethiol (DDT), 1-octadecanethiol (ODT), 4-mercaptobenzoic acid (MBA), 4-aminothiophenol (4-ATP), 5,5′-dithiobis(2-nitrobenzoic acid) (DTNB), 4-mercaptophenylboronic acid (MPBA), tween-20, rhodamine 6 G (R6 G), basic red 9 (BR9) and thiabendazole were purchased from Sigma-Aldrich Inc. (USA). Ethanol, N,*N*-dimethylformamide (DMF), hydrochloric acid (HCl), ethylenediamine tetraacetic acid (EDTA), tris(hydroxymethyl)amino-methane, $FeCl_3 \cdot 6H_2O$, NaCl and $NaHCO_3$ were obtained from Sinopharm Chemical Reagent Co., Ltd (China). Benzonitrile (BN) were purchased from Adamas-beta (China). Tris-EDTA buffer contained 10 mM Tris − HCl and 1 mM EDTA (pH 7.40, containing 0.005% tween-20). Apples were obtained from the local market. All reagents were of analytical grade and all aqueous solutions were prepared using ultrapure water (18 MΩ, Milli-Q, Millipore).

2.2. Apparatus

The transmission electron microscopic (TEM) and scanning electron microscopic (SEM) images were gained on a JEM-2100 transmission electron microscope (JEOL Ltd., Japan) and S-4800 scanning electron microscope (HITACHI, Japan) equipped with an energy dispersive X-ray (EDX) spectroscopic facility, respectively. The TEM images were analyzed by Image *J* software. The dynamic light scattering (DLS) measurement was performed on a 90 Plus / BI-MAS equipment (Brook haven, USA). The UV–vis absorption spectra were recorded on a UV-3600 UV-VIS-NIR spectrophotometer (SHIMADZU, Japan), and the morphology of the device was observed under an Agilent 5500 atomic force microscope (AFM, USA). The spin-coating and drying of PMMA were performed on a spin coater and hot plate, respectively (SETCAS Electronics Co., Ltd, China). The fabrication of AuNS@1LG foil was performed on a TMS-300 temperature-controlled vibrator (Hangzhou Allsheng instruments Co., Ltd, China). Raman spectra were recorded on a Renishaw inVia confocal Raman microscope (Renishaw, UK). 50 × and 20 × telephoto objectives were used for optical images and spectral measurements. All the data were analyzed with WiRE 3.4 and Origin 8.0 software.

2.3. Synthesis of AuNSs and gold nanoflowers (AuNFs)

The synthesis of AuNSs was based on the previous study [24]. Firstly, the 15 nm PVP-coated gold seeds were prepared by rapidly adding 5 mL trisodium citrate (1% wt) into 100 mL boiling $HAuCl_4$ solution (0.5 mM) to react for 15 min. After the mixture was cooled to room temperature, 8.6 mL PVP (25.6 g/L, MW = 10,000) was added dropwise and allowed to stand overnight. The gold seeds were rinsed with ethanol by centrifugation (4000 rpm, 90 min) and redispersed. The concentration of the dispersion was determined using UV–vis absorption spectrometry [25]. The AuNSs were then synthesized by adding 43 μL above gold seeds (4.2 mM) into 15 mL DMF solution containing $HAuCl_4$ (0.3 mM) and PVP (10 mM) under rapid stirring for 15 min. The resulting AuNSs were washed by centrifugation (6000 rpm, 10 min) and redispersed in ethanol.

AuNFs were synthesized according to previous work [26]. 1.0 mL $HAuCl_4$ solution (1% wt) was quickly added to 50 mL HEPES (10 mM, pH 7.4) under continuous stirring at room temperature until the color of solution turned to turbid blue. Afterward, AuNFs were washed by centrifugation (5000 rpm, 15 min) and resuspended in ultrapure water containing 0.005% wt tween-20.

2.4. Preparation of AuNSs@1LG foil and AuNFs@1LG foil

The 1LG Cu foil was cut into a suitable size, cleaned with nitrogen flow and then vertically immersed into 1 mM ethanol solution of DDT for one hour under room temperature. Afterward, the foil was air-dried and then rinsed in water, followed by cleaning with nitrogen flow. The as-prepared foil was vertically immersed into the AuNS solution (1 nM, in ethanol). After incubation in a vibrator under 43 ℃ and 350 rpm for 18 h, the AuNSs@1LG foil was taken out, rinsed in water and then cleaned with nitrogen flow. The foil could be stored in air for over one week without any change. The AuNSs@1LG foil was also prepared with ODT by replacing DDT with ODT. The AuNFs@1LG foil was prepared with the same procedure except for replacing AuNSs with AuNFs.

2.5. Fabrication of GAGD

GAGD was the combination of the AuNSs@1LG foil (the SERS-active module) and one piece of internal standard (IS) adsorbed 1LG protected with PMMA membrane (the IS module). The latter was prepared with following procedure: Firstly, 1LG Cu foil was cleaned with nitrogen flow and vertically immersed into 10 mM ethanol solution of MBA as the IS for one hour under room temperature. After air-dried, the foil was rinsed with water gently and then cleaned with nitrogen flow. Subsequently, 2% PMMA was spin-coated (2000 rpm, 60 s) on the MBA-adsorbed graphene via the van der Waals interactions between PMMA and graphene. After the PMMA was dried on a hot plate (120 ℃, 5 min), the Cu substrate on another side of the graphene was etched in $FeCl_3$ (1 M) for 5 h by the traditional PMMA-mediated method [27] and the obtained IS adsorbed 1LG membrane was rinsed with 1:4 HCl and ultrapure water in sequence for further assembly. Other IS adsorbed 1LG

membranes were also prepared with different IS (4-ATP, DTNB, BN, MPBA). Finally, the membrane as the IS module was transferred onto the surface of as-prepared AuNSs@1LG foil (or AuNFs@1LG foil). After air-dried and then spin-coating with 2% PMMA on the upper side, the Cu substrate was etched in $FeCl_3$ (1 M) for 5 h to obtain the GAGD for SERS detection. The AuNFs-based GAGD was prepared with the same procedure except for replacing AuNSs@1LG foil with AuNFs@1LG foil.

As comparison, the 1LG@AuNSs-MBA@1LG composite was fabricated as following: 1 nM AuNS solution was mixed with 100 μM MBA in ethanol overnight. After washing by centrifugation, the AuNSs-MBA solution was used to immerse the 1LG Cu foil treated with DDT. After incubation in a vibrator under 43 ℃ and 350 rpm for 18 h, the AuNSs-MBA@1LG foil was taken out, rinsed in water and cleaned with nitrogen flow. Meanwhile, one piece of 1LG protected with PMMA membrane was prepared by spin-coating 2% PMMA (2000 rpm, 60 s) on 1LG Cu foil and etching the Cu foil in $FeCl_3$ (1 M) for 5 h. After the 1LG membrane was transferred on the AuNSs-MBA@1LG foil, the PMMA membrane was spin-coated, and the Cu foil was etched in $FeCl_3$ (1 M) again to obtain the 1LG@AuNSs-MBA@1LG composite. Similarly, 1LG@1LG-MBA composite was also prepared.

2.6. Raman measurements

After the device was floated on the sample solution with the IS side facing up and the lower 1LG contacting with target, the SERS spectra of the IS and the target were collected with exposure time of 10 s and laser power of 5.0 mW under 633 nm. The relative intensity of the target characteristic peak to IS characteristic peak at 1075 cm^{-1} was used to quantitate the target concentration with a standard curve method. Using R6 G as the target mode, its characteristic peak occurred at 1508 cm^{-1}. As comparison, the SERS spectrum of R6 G adsorbed AuNSs was also recorded, which was prepared by mixing 1 nM AuNSs with 1 mM R6 G in TE buffer containing 0.5 M/1.0 M Na^+ for 1 h under room temperature, and dropping the mixture on a glass slide for SERS measurments.

When the device was used for imaging the distribution of target on sample surface, it was held by a tweezer to directly place on sample surface for collecting the SERS spectra of the IS and the target with 20 × times telephoto objective, the exposure time of 1 s and laser power of 50 mW under 785 nm. As the proof-of-concept, apple samples were treated by 1000 or 200 ppm thiabendazole aqueous solution for testing. The SERS imaging area was 200 μm × 200 μm, and data were collected using signal to baseline map review mode from 1035 cm^{-1} to 1105 cm^{-1} for IS and 1250 cm^{-1} to 1310 cm^{-1} for thiabendazole. The residue was also detected after washing the apple with 10 mg/mL $NaHCO_3$ solution for 150 s.

The device could be regenerated by a washing step with ethanol, which was performed by holding the GAGD with a silicon wafer and gently vibrating the wafer in ethanol for 5 s. Afterward the device could be reused for the sample detection.

2.7. Finite-difference time domain (FDTD) simulation of GAGD

The FDTD simulation was performed on a commercial FDTD software package Lumerical@FDTD Solution 8.6. The AuNS model was 30 nm in radius and had 14 points around core, which was referred to the TEM images. In order to simulate GAGD structure, the dimer of AuNSs was placed between two pieces of 1LG. Two kinds of plane wave were used as the excitation source of 633 and 785 nm in wavelength propagated along Y-axis, and the polarization was along X-axis. The simulation object had periodic boundary conditions in X-axis and Z-axis and PML boundary condition in Y-axis. Note that the mesh size around corners and interaction area was 1 nm, and cross section view of simulation region was monitored from X–Y plane.

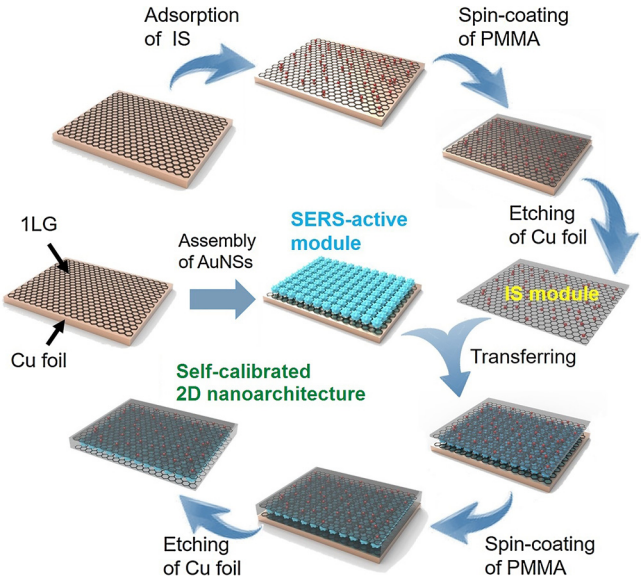

Fig. 1. Manufacture of self-calibrated 2D Nanoarchitecture.

3. Results and discussion

3.1. Fabrication and morphological characterization of GAGD

As proof-of-concept, AuNSs, which owns outstanding SERS performance [28–30], and 1LG were used to construct the GAGD by combining two designed modules (Fig. 1). Firstly, the monolayer of AuNSs was self-assembled on the surface of 1LG foil with DDT as a linkage to obtain the "SERS-active module" (Fig. S1A), denoted as AuNSs@1LG foil. The AuNSs used in the fabrication were highly uniform and showed numerous sharp tips (Fig. S2A). The multibranched structure (Fig. S2B) was very favorable to SERS application [31]. Their core diameter was 60.0 ± 5.7 nm, and the tip radius of curvature was measured to be 2.9 ± 0.6 nm (Figs. S2C and S2D). The DLS and UV–vis spectroscopic measurements (Figs. S2E and S2F) further conformed the uniformity and multibranched structure, respectively [24]. More importantly, the AuNSs showed low SERS background (Fig. S3), thus were good SERS substrates for analytical application. The Raman spectrum of CVD-grown 1LG showed negligible D band related to a series of defects around 1355 cm^{-1} (Fig. S4), indicating its high quality with non-oxidative property.

After DDT was self-assembled on the surface of 1LG Cu foil, the EDX spectrum showed the existence of thiol (Fig. S1A). Thus the DDT modified 1LG Cu foil could further assemble the AuNSs on the foil surface by incubating the AuNS solution under 43 ℃ with a vibration rate of 350 rpm (Fig. S5). The assembled AuNSs showed a dense monolayer and maintained their typical multibranched structure (Figs. S1B–1D). The EDX spectrum also demonstrated the thiol-induced assembly of AuNSs, which led to the appearance of Au peak (Fig. S1A). When ODT was used as an alternative linkage to perform the self-assembly of AuNSs on 1LG Cu foil, the obtained AuNSs@1LG foil also showed similar morphology (Fig. S6), indicating the feasibility of the procedure.

The other module was denoted as "IS module", which was fabricated with another piece of 1LG to import IS onto GAGD via π-π interaction between MBA as the IS and graphene (Fig. 1). After the IS module was transferred onto SERS-active module with a conventional wet transferring method, the whole architecture was further immobilized by spin-coating PMMA to obtain an IS-implanted 1LG-AuNSs-1LG foil (Fig. 2A). The Cu foil was then dissolved with $FeCl_3$ solution to obtain the GAGD, which could float on the water due to its ultra-thin and freestanding 2D structure (Fig. 2B). The slightly different dispersity

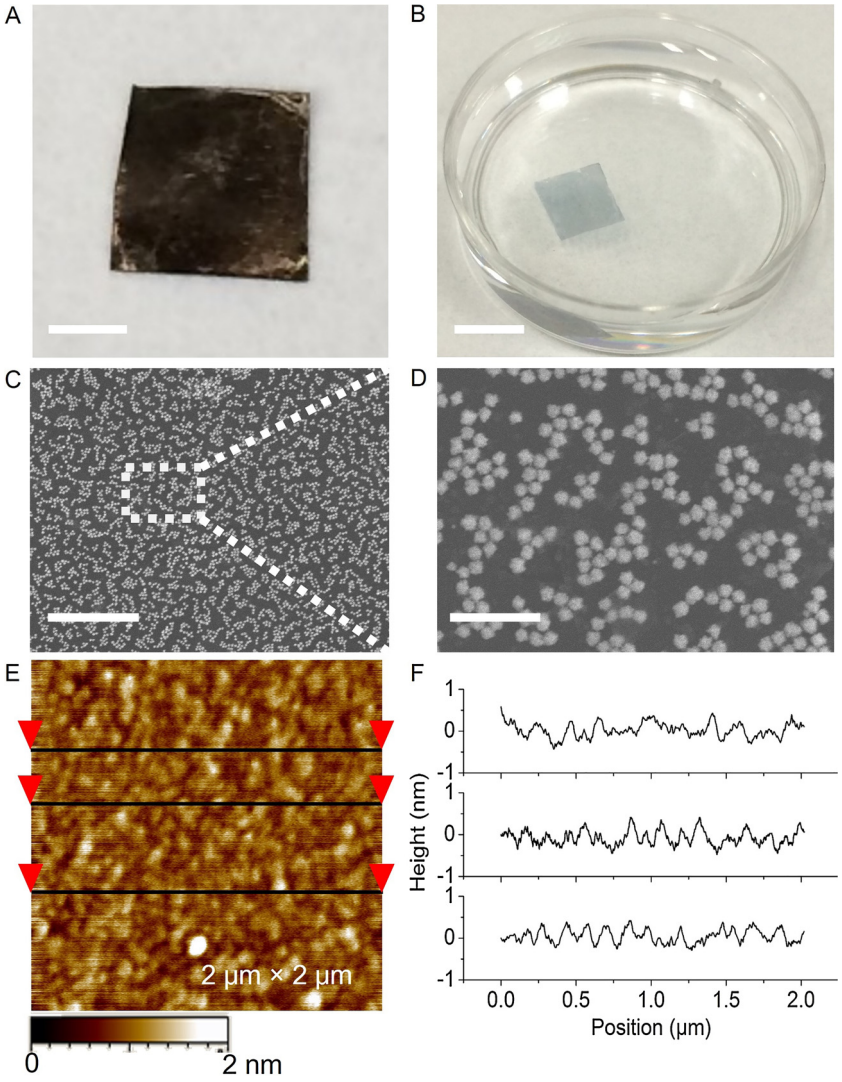

Fig. 2. Optical images of (A) IS-implanted 1LG-AuNSs-1LG foil coated with PMMA membrane (scale bar: 2 mm) and (B) GAGD floated on water (scale bar: 5 mm). SEM images of GAGD at scale bars of (C) 2 μm and (D) 500 nm. (E) AFM image of GAGD, and (F) height profile of the three black lines from top to bottom in E.

and density of AuNSs monolayer inside GAGD (Fig. 2C and D) from the AuNSs@1LG foil (Figs. S1C and S1D) should be mainly attributed to the different batches of SERS-active module prepared on different graphene sheets. The broad absorbance band in UV–vis spectrum indicated the multibranched structure of AuNSs sandwiched between two pieces of graphene in the PMMA membrane (Fig. S7). The AFM image confirmed dense and uniform distribution of AuNSs without stacking (Fig. 2E). The height profiles of gold nanostars in three sections showed similar height fluctuation (Fig. 2F) with the relative standard deviation (RSD) for 20 height measurements of 17.2%, 17.2% and 15.8%, respectively, further indicating the uniform distribution of AuNSs inside GAGD. These features assured the form of a huge number of hot spots for efficient SERS detection.

3.2. SERS features of GAGD

The SERS spectra of GAGD in both presence and absence of IS showed negligible D band around 1355 cm^{-1} (Fig. 3A). Thus the fabrication process did not bring any defect to 1LG. In the presence of IS, the SERS spectrum showed two new strong peaks at 1075 cm^{-1} and 1588 cm^{-1}, which was attributed to the ν_{CC} and $\nu_{CC' + CC}$ vibrations of MBA molecule [32,33]. Compared to the Raman spectrum of 1LG@1LG-MBA (similar nanoarchitecture without presence of AuNS monolayer), which showed very weak peaks of MBA (Fig. S8), it could be concluded that the AuNSs rather than 1LG in GAGD played a major role in Raman enhancement. Furthermore, the strong SERS peaks could be observed under both 633 and 785 nm excitation (Fig. 3B), which meant that GAGD could work at two different excitation conditions. In addition, the SERS spectra of GAGD at 12 randomly selected spots showed similar peak intensity of IS (Fig. 3C). Their RSD at 1075 cm^{-1} was 9.4% (Fig. 3D), representing acceptable Raman enhancement uniformity and reproducibility. The IS signal of GAGD also showed a good duration stability against photobleaching (or photodegradation) induced by continuous laser irradiation, which was evaluated by recording the SERS spectra in a time series of 600 s at the same spot and gave a RSD of only 4.6% (Fig. 3E and F). Under the excitation wavelength of 785 nm, GAGD also showed similar signal uniformity and duration stability with the RSD of 8.4% and 5.4%, respectively (Fig. S9). After the device was floated on water at room temperature for six months, the IS signal kept relatively stable (Fig. S10), indicating excellent long-term stability of the GAGD. Both uniformity and the good stability were attributed to the sealed sandwich structure that separated the AuNSs and IS from the test environment, homogeneous GAGD structure, the separation of MBA from the AuNS surface and the strong interaction between MBA and 1LG.

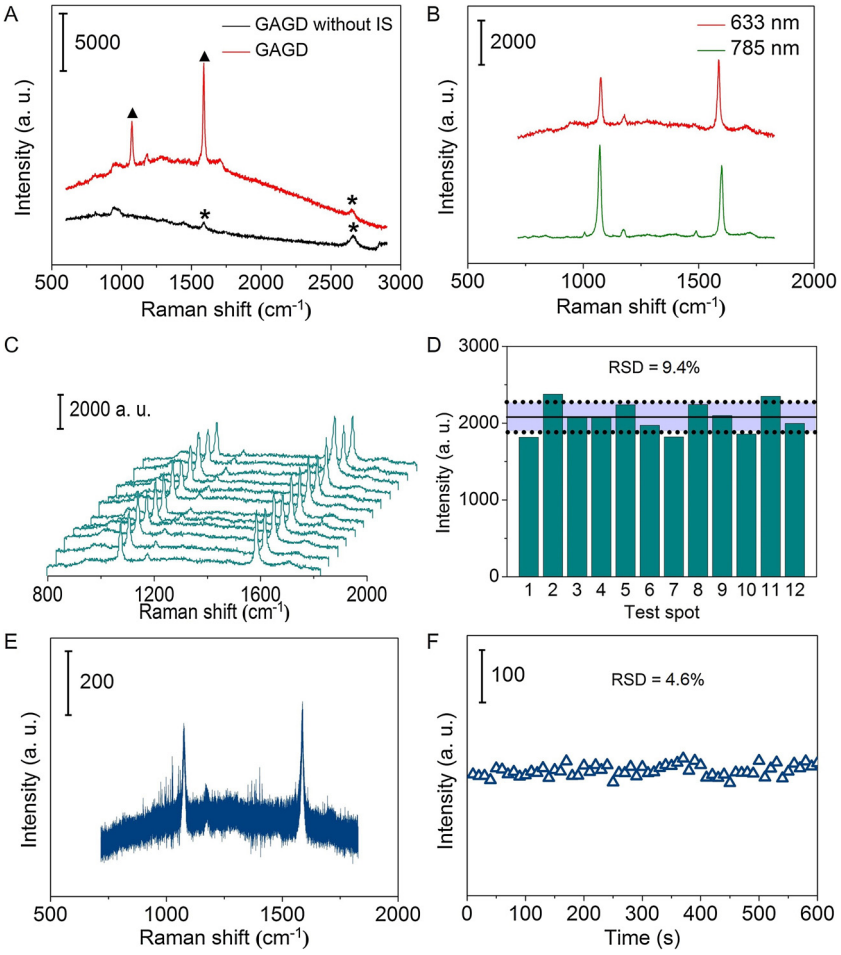

Fig. 3. SERS spectra of (A) GAGD with and without IS excited at 633 nm and (B) GAGD excited at 633 and 785 nm with exposure time of 10 s. The black triangles and asterisks marked characteristic peaks from IS and 1LG, respectively. (C) SERS spectra of GAGD and (D) peak intensities at 1075 cm^{-1} at 12 randomly selected spots in 160 μm × 120 μm area with exposure time of 10 s. (E) SERS spectra of GAGD and (F) peak intensities at 1075 cm^{-1} in continuous laser irradiation for 600 s with the measurement time of 1 s and interval of 10 s at one spot. Laser power: 5.0 mW at 633 nm for (C)–(F).

3.3. Extensibility of GAGD

Due to the π-π interaction of graphene with different types of molecules, the GAGD possessed diversified structure collocation in choosing the IS. When other molecules, such as 4-ATP, DTNB, MPBA and BN, were adsorbed on 1LG Cu foil for GAGD fabrication, all resulting GAGDs showed their SERS peaks (Fig. 4). Thus these molecules could also be considered as the IS for different analytes. Furthermore, the GAGD could be prepared with other kinds of gold nanoparticles. For instance, a similar nanoarchitecture constructed with AuNFs displayed highly versatile property of this design (Fig. S11).

3.4. SERS quantitative ability of GAGD

In order to verify the quantitative ability of the GAGD with SERS technology, R6 G was used as a model target. After the GAGD was directly floated on R6 G solution (Fig. 5A), the Raman spectrum showed strong and distinct SERS peaks of R6 G at 1128, 1182, 1310, 1362, 1508 and 1648 cm^{-1} [34] and MBA at 1075 and 1588 cm^{-1}. The signals of target and IS did not disturb each other (Fig. 5B). The Raman peaks of R6 G were almost invisible in the absence of substrates, while the presence of 1LG@1LG-MBA led to obvious Raman response due to the chemical enhancement from GERS. However, 1LG@1LG-MBA floated on 1 mM R6 G showed much weaker SERS signals of R6G than GAGD (Fig. 5B), which indicated the contribution of AuNSs on SERS signals due to their electromagnetic enhancement. Moreover, the fluorescent background of R6G did not affect its Raman response due to the presence of graphene inside GAGD, which can generally quench the fluorescence through energy transfer. At high concentrations of Na^+, the GAGD showed clear SERS peaks of target (Fig. S12), indicating it was suitable to high-salt environment. This feature was obviously superior to pure AuNSs as SERS substrate, which produced serious sedimentation at high salt concentrations and thus led to the invisibility of SERS peaks (Fig. S12). In addition, the GAGD could be regenerated by a simple washing step, which did not show remarkable change of SERS signal after it was reused for five cycles (Fig. S13) due to the assistance of 1LG as a protective barrier and its freestanding character.

With the increasing R6 G concentration, its SERS peak intensity increased, while the intensity of MBA showed ignorable change (Fig. 5C). The relative intensity of R6 G at 1508 cm^{-1} to MBA as the IS at 1075 cm^{-1} perfectly followed the Langmuir-type relativity (R^2 = 0.9910) due to the adsorption of R6 G on 1LG surface of the GAGD. A linear plot could be observed in the range of 0–8.0 μM (R^2 = 0.9950) (Fig. 5D). Obviously, the plot of raw SERS intensity of R6 G vs its concentration showed poor correlation with larger error bars (Fig. S14), indicating that the presence of IS greatly improved the quantitative ability.

The mechanism for efficient IS-calibration was investigated by building a model with FDTD method under 633 and 785 nm excitation (Fig. S15). Since the Raman cross-section enhancement is proportional to the fourth power of the field enhancement ($|E|^4$), it was clear that the hot spots were produced from the sharp tips of AuNSs, which located at

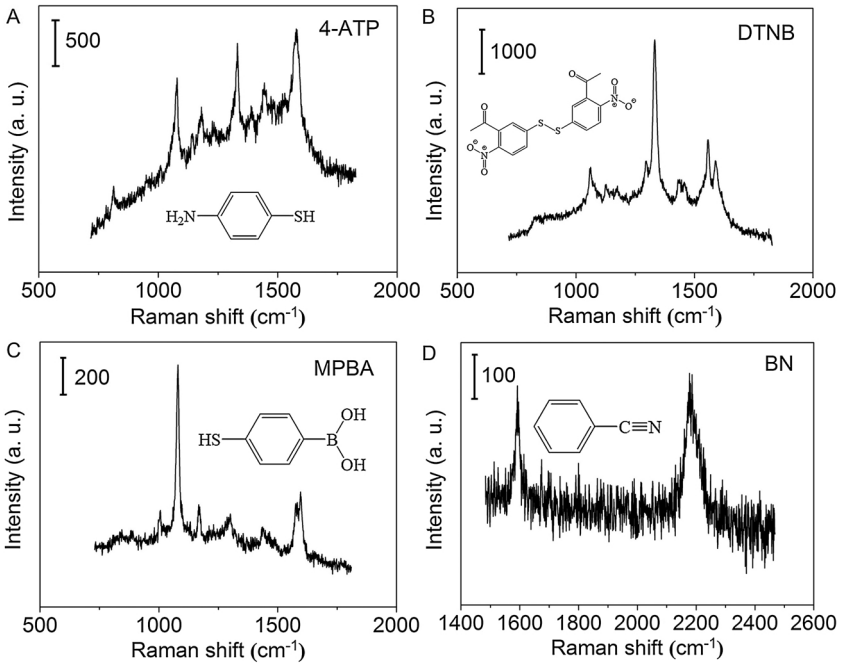

Fig. 4. SERS spectra of GAGDs with marked IS at exposure time of 10 s under laser power of (A, B and C) 5.0 mW at 633 nm and (D) 50 mW at 785 nm.

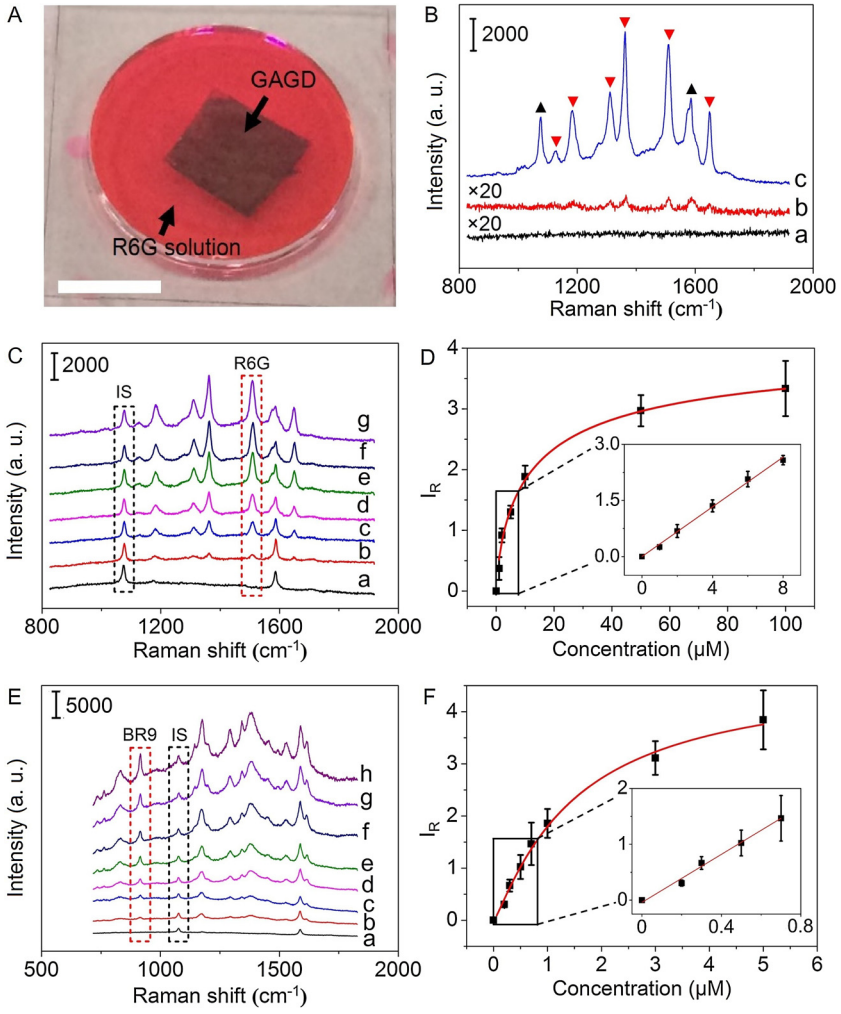

Fig. 5. (A) Optical image of GAGD floated on R6 G solution. Scale bar: 5 mm. (B) Raman spectrum of 1 mM R6 G (a), and SERS spectra of 1LG@1LG-MBA (b) and GAGD (c) floated on 1 mM R6G solution. The black triangles and red inverted triangles marked characteristic peaks from IS and R6 G, respectively. (C) SERS spectra of GAGD floated on 0, 1.0, 2.0, 5.0, 10, 50 and 100 μM R6 G (a–g) and (D) plot of relative SERS intensity vs R6 G concentration. (E) SERS spectra of GAGD floated on 0, 0.2, 0.3, 0.5, 0.7, 1.0, 3.0 and 5.0 μM BR9 (a–h) and (F) plot of relative SERS intensity vs BR9 concentration. The peaks used in quantification were marked in (C) and (E). All SERS spectra are measured with exposure time of 10 s under laser power of 5.0 mW at 633 nm. The error bars are from 10 and 5 measurements with different GAGDs for R6D and BR9, respectively. (For interpretation of the references to colour in this figure legend, the reader is referred to the web version of this article.)

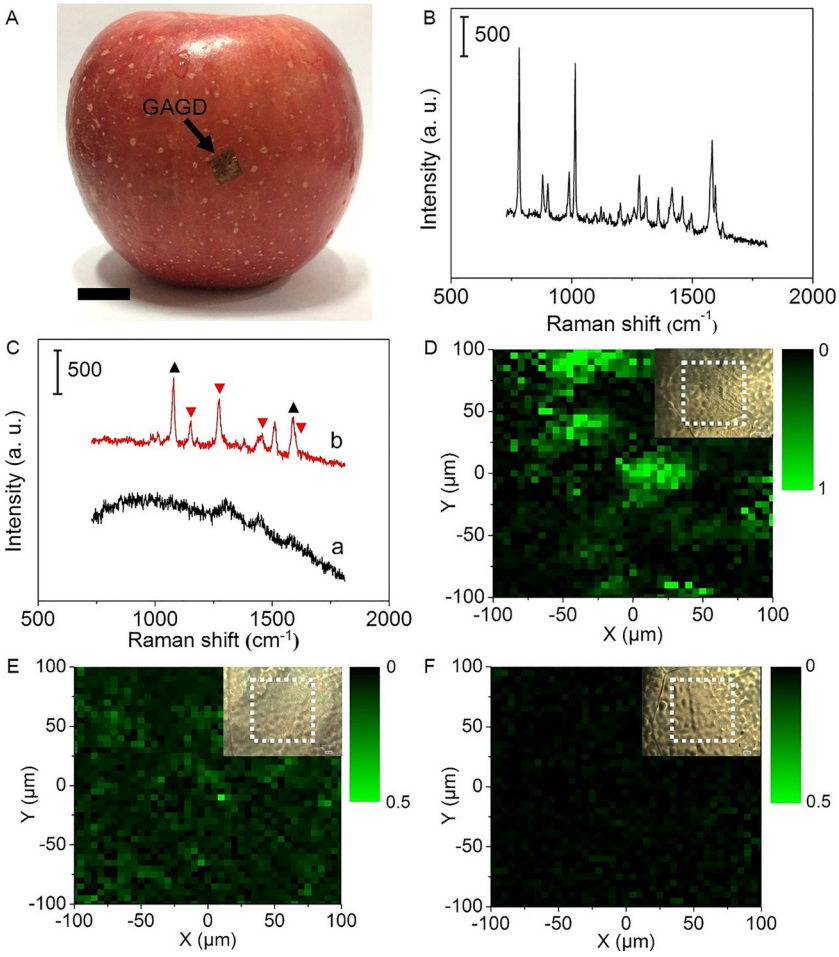

Fig. 6. (A) Optical image of GAGD attached on apple surface. Scale bar: 10 mm. (B) Raman spectrum of pure thiabendazole. (C) Raman (a) and SERS (b) spectra, and (D) SERS imaging of apple surface treated with 1000 ppm thiabendazole (The optical image of imaging area was marked by white frame). (E,F) SERS imaging of the apple treated with 200 ppm thiabendazole (E) before and (F) after vibration washing with 10 mg/mL $NaHCO_3$ solution for 150 s. Black triangles and red inverted triangles in (C) marked characteristic peaks from IS and thiabendazole, respectively. All spectra are measured with exposure time of 1 s under laser power of 50 mW at 785 nm, and imaging data are collected with signal to baseline map review mode from 1035 cm^{-1} to 1105 cm^{-1} for IS and 1250 cm^{-1} to 1310 cm^{-1} for thiabendazole. (For interpretation of the references to colour in this figure legend, the reader is referred to the web version of this article.)

both upper surface (IS location) and lower surface (target location) across the 1LG (Figs. S15A and S15B). Therefore, the target and IS can both enjoyed the SERS environment on GAGD surface due to the vertical irradiation of the laser on GAGD, and the SERS signal of IS can be used to correct for effects such as the instrumental factors and differences in focus due to substrate morphology [12]. Furthermore, the electromagnetic hot spots on upper and lower surface of GAGD could permeate the 1LG and showed stronger electromagnetic enhancement value of $|E|^4$ (Table S1) (Figs. S15C and S15D), which implied the contribution of 1LG to Raman enhancement and realization of hot surface at atomically flat level [5].

In addition, when the IS was directly loaded on AuNS surface, the formed 1LG@AuNS-MBA@1LG nanoarchitecture expressed relatively inferior uniformity of IS signal (RSD = 15.3%, Fig. S16A), compared with the GAGD (Fig. 3D), and the linear relativity was also worse (R^2 = 0.9720, Fig. S16B). Thus the superior quantitative ability also resulted from the presence of 1LG for even dispersion of target and IS on the surface.

3.5. SERS quantitation of target in liquid sample

The quantitative detection capability for liquid sample was demonstrated by analyzing the water contaminant BR9, a carcinogenic dyestuff forbidden in textile industry. Similarly, the BR9 aqueous solution showed the SERS characteristic peaks of BR9 at 830, 915, 1175, 1292, 1380, 1530 and 1613 cm^{-1} (Fig. 5E) [4]. The plot of relative intensity of the peak at 915 cm^{-1} to IS at 1075 cm^{-1} also perfectly followed the Langmuir-type relativity (R^2 = 0.9930) and a linear plot could be observed in the range of 0 to 0.7 μM (R^2 = 0.9906). This provided a quantitative method for convenient rapid detection of BR9 with a linear calibration and a limit of detection (LOD) of 79 nM at 3 times standard deviation of blank signal (Fig. 5F), which were much lower than the detection limit of international OEKO-TEX® Standard 100 of BR9. The detection could be completed within 1 min, indicating the potential of the GAGD in fast detection.

3.6. In situ SERS imaging of target distribution on solid surface

The 2D nanoarchitecture also showed superior in situ SERS imaging performance of real solid sample. Due to the excellent flexibility and ultra-thin thickness of the GAGD, it could be easily attached on solid surface for imaging the distribution of target on sample surface (Fig. 6A). As a proof-of-concept, this protocol was used for fungicide residue imaging on apple surface. Using thiabendazole, an extensively used fungicide in agriculture [35], as a target model, the apple samples were firstly immersed into 200 or 1000 ppm thiabendazole, which simulated actual situation for sterilization treatments in agriculture. Considering the strong self-fluorescence of plant tissue excited under 633 nm, a laser of 785 nm was used for SERS measurements, at which the thiabendazole showed the Raman peaks at 1156, 1279, 1460 and 1595 cm^{-1} (Fig. 6B). The GAGD attached on thiabendazole treated apple also showed these characteristic peaks, while these peaks were not observed in the absence of GAGD (Fig. 6C). Using the SERS peak at 1274 cm^{-1} to collect the imaging data of thiabendazole and the SERS peak of IS at 1075 cm^{-1} as calibration, the SERS imaging of the treated apple showed the clear surface distribution of thiabendazole (Fig. 6D). The signals were related to the distributed amount of thiabendazole on apple surface. The apple treated with 200 ppm thiabendazole showed lower signals (Fig. 6E). Upon a vibration washing step with 10 mg/mL $NaHCO_3$ solution for 150 s [36], these signals almost disappeared,

indicating effective removing of thiabendazole (Fig. 6F). Interestingly, the quality of SERS imaging obviously depended on the IS calibration. The imaging without IS calibration showed relatively dispersive and messy information (Fig. S17). This resulted from the highly uneven surface of apple (Fig. S18), which could not provide a constant focal position for SERS measurements and thus eventually disturbed the signal collection. The ultra-thin GAGD structure along with the IS calibration effectively eliminated the influence of uneven surface on surface imaging. In addition, the imaging measurement could be completed within 1 h. These performance manifested that GAGD was a powerful tool for fast in situ SERS imaging analysis.

4. Conclusion

This work designs a self-calibrated 2D nanoarchitecture as a sensing device for SERS quantitation and imaging. This device can be reproducibly fabricated with AuNSs and two pieces of commercial 1LG Cu foils, which implants IS onto one side of the device and detects the target on the opposite side. The AuNS monolayer leads to highly sensitive SERS signals, and the presence 1LG assures the stable and reproducible SERS signals. Moreover, the separation of IS and target on two sides of the GAGD avoids the competition of IS with target molecules to the surface adsorption sites. Thus, the distinct SERS signals from both IS and target in/on the sample can be easily collected for reliable quantification and imaging. The ultra-thin structure and excellent flexibility make it applicable to arbitrary target detection by conveniently floating on solution or covering on solid surface for convenient SERS measurements without any pretreatment. Considering the outstanding stability, reusability, durability and the flexibility in choosing inner IS and SERS substrate, this nanoarchitecture provides a powerful tool for fast and portable SERS quantitative and imaging analysis of a wide variety of samples. This strategy can also be extended to construct wearable sensing device for future analytical studies, especially point-of-care testing (POCT).

Acknowledgements

We gratefully acknowledge National Natural Science Foundation of China (21635005, 21361162002, 21605080) and Natural Science Foundation of Jiangsu Province (BK20160646).

Appendix A. Supplementary data

Supplementary material related to this article can be found, in the online version, at doi:https://doi.org/10.1016/j.snb.2018.06.029.

References

[1] S.M. Nie, S.R. Emory, Probing single molecules and single nanoparticles by surface-enhanced Raman scattering, Science 275 (1997) 1102–1106.
[2] J.F. Li, Y.F. Huang, Y. Ding, Z.L. Yang, S.B. Li, X.S. Zhou, F.R. Fan, W. Zhang, Z.Y. Zhou, D.Y. Wu, B. Ren, Z.L. Wang, Z.Q. Tian, Shell-isolated nanoparticle-enhanced Raman spectroscopy, Nature 464 (2010) 392–395.
[3] S. Schlücker, Surface-enhanced Raman spectroscopy: concepts and chemical applications, Angew. Chem. Int. Ed. 53 (2014) 4756–4795.
[4] W. Shen, X. Lin, C.Y. Jiang, C.Y. Li, H.X. Lin, J.T. Huang, S. Wang, G.K. Liu, X.M. Yan, Q.L. Zhong, B. Ren, Reliable quantitative SERS analysis facilitated by core–shell nanoparticles with embedded internal standards, Angew. Chem. Int. Ed. 54 (2015) 7308–7312.
[5] W.G. Xu, X. Ling, J.Q. Xiao, M.S. Dresselhaus, J. Kong, H.X. Xu, Z.F. Liu, J. Zhang, Surface enhanced Raman spectroscopy on a flat graphene surface, Proc. Natl. Acad. Sci. U. S. A. 109 (2012) 9281–9286.
[6] X.Y. Zhang, Y.H. Zheng, X. Liu, W. Lu, J.Y. Dai, D.Y. Lei, D.R. MacFarlane, Hierarchical porous plasmonic metamaterials for reproducible ultrasensitive surface-enhanced Raman spectroscopy, Adv. Mater. 27 (2015) 1090–1096.
[7] X. Liu, S. Lebedkin, H. Besser, W. Pfleging, S. Prinz, M. Wissmann, P.M. Schwab, I. Nazarenko, M. Guttmann, M.M. Kappes, U. Lemmer, Tailored surface-enhanced Raman nanopillar arrays fabricated by laser-assisted replication for biomolecular detection using organic semiconductor lasers, ACS Nano 9 (2015) 260–270.
[8] S.R. Si, W.K. Liang, Y.H. Sun, J. Huang, W.L. Ma, Z.Q. Liang, Q.L. Bao, L. Jiang, Facile fabrication of high-density sub-1-nm gaps from Au nanoparticle monolayers as reproducible SERS substrates, Adv. Funct. Mater. 26 (2016) 8137–8145.
[9] Z.B. Li, G.W. Meng, Q. Huang, C. Zhu, Z. Zhang, X.D. Li, Galvanic-cell-induced growth of Ag nanosheet-assembled structures as sensitive and reproducible SERS substrates, Chem. Eur. J. 18 (2012) 14948–14953.
[10] R.W. Taylor, T.C. Lee, O.A. Scherman, R. Esteban, J. Aizpurua, F.M. Huang, J.J. Baumberg, S. Mahajan, Precise subnanometer plasmonic junctions for SERS within gold nanoparticle assemblies using cucurbit[*n*]uril "glue", ACS Nano 5 (2011) 3878–3887.
[11] S. Kasera, F. Biedermann, J.J. Baumberg, O.A. Scherman, S. Mahajan, Quantitative SERS using the sequestration of small molecules inside precise plasmonic nanoconstructs, Nano Lett. 12 (2012) 5924–5928.
[12] S.E.J. Bell, N.M.S. Sirimuthu, Quantitative surface-enhanced Raman spectroscopy, Chem. Soc. Rev. 37 (2008) 1012–1024.
[13] Y. Zhou, R. Ding, P. Joshi, P. Zhang, Quantitative surface-enhanced Raman measurements with embedded internal reference, Anal. Chim. Acta 874 (2015) 49–53.
[14] P. Joshi, Y. Zhou, T.O. Ahmadov, P. Zhang, Quantitative SERS-based detection using Ag-Fe_3O_4 nanocomposites with an internal reference, J. Mater. Chem. C 2 (2014) 9964–9968.
[15] Y.X. Zou, L. Chen, Z.L. Song, D. Ding, Y.Q. Chen, Y.T. Xu, S.S. Wang, X.F. Lai, Y. Zhang, Y. Sun, Z. Chen, W.H. Tan, Stable and unique graphitic Raman internal standard nanocapsules for surface-enhanced Raman spectroscopy quantitative analysis, Nano Res. 9 (2016) 1418–1425.
[16] Y. Zhang, J. Li, H. Liang, L. Chen, Z. Chen, W.H. Tan, Stable graphene-isolated-Au-nanocrystal for accurate and rapid surface enhancement Raman scattering analysis, Anal. Chem. 88 (2016) 10611–10616.
[17] P. Matteini, M. Cottat, F. Tavanti, E. Panfilova, M. Scuderi, G. Nicotra, M.C. Menziani, N. Khlebtsov, M. Angelis, R. Pini, Site-selective surface-enhanced Raman detection of proteins, ACS Nano 11 (2016) 918–926.
[18] D. Kurouski, M. Sorci, T. Postiglione, G. Belfort, I.K. Lednev, Detection and structural characterization of insulin prefibrilar oligomers using surface enhanced Raman spectroscopy, Biotechnol. Prog. 30 (2014) 488–495.
[19] W.G. Xu, N.N. Mao, J. Zhang, Graphene: a platform for surface-enhanced Raman spectroscopy, Small 9 (2013) 1206–1224.
[20] N. Zhang, L.M. Tong, J. Zhang, Graphene-based enhanced Raman scattering toward analytical applications, Chem. Mater. 28 (2016) 6426–6435.
[21] S.X. Huang, X. Ling, L.B. Liang, Y. Song, W.J. Fang, J. Zhang, J. Kong, V. Meunier, M.S. Dresselhaus, Molecular selectivity of graphene-enhanced Raman scattering, Nano Lett. 15 (2015) 2892–2901.
[22] W.G. Xu, J.Q. Xiao, Y.F. Chen, Y.B. Chen, X. Ling, J. Zhang, Graphene-veiled gold substrate for surface-enhanced Raman spectroscopy, Adv. Mater. 25 (2013) 928–933.
[23] H.W. Qiu, M.Q. Wang, S.Z. Jiang, L. Zhang, Z. Yang, L. Li, J.J. Li, M.H. Cao, J. Huang, Reliable molecular trace-detection based on flexible SERS substrate of graphene/Ag-nanoflowers/PMMA, Sens. Actuators B Chem. 249 (2017) 439–450.
[24] P.S. Kumar, I. Pastoriza-Santos, B. Rodríguez-González, F.J.G. Abajo, L.M. Liz-Marzán, High-yield synthesis and optical response of gold nanostars, Nanotechnology 19 (2008) 015606.
[25] W. Haiss, N.T.K. Thanh, J. Aveyard, D.G. Fernig, Determination of size and concentration of gold nanoparticles from UV-Vis spectra, Anal. Chem. 79 (2007) 4215–4221.
[26] J.P. Xie, Q.B. Zhang, J.Y. Lee, D.I.C. Wang, The synthesis of SERS-active gold nanoflower tags for in vivo applications, ACS Nano 2 (2008) 2473–2480.
[27] L.Y. Jiao, B. Fan, X.J. Xian, Z.Y. Wu, J. Zhang, Z.F. Liu, Creation of nanostructures with poly(methyl methacrylate)-mediated nanotransfer printing, J. Am. Chem. Soc. 130 (2008) 12612–12613.
[28] W.X. Niu, Y.A.A. Chua, W.Q. Zhang, H.J. Huang, X.M. Lu, Highly symmetric gold nanostars: crystallographic control and surface-enhanced Raman scattering property, J. Am. Chem. Soc. 137 (2015) 10460–10463.
[29] L. Rodríguez-Lorenzo, R.A. Álvarez-Puebla, I. Pastoriza-Santos, S. Mazzucco, O. Stéphan, M. Kociak, L.M. Liz-Marzán, F.J.G. Abajo, Zeptomol detection through controlled ultrasensitive surface-enhanced Raman scattering, J. Am. Chem. Soc. 131 (2009) 4616–4618.
[30] S. Carrasco, E. Benito-Peña, F. Navarro-Villoslada, J. Langer, M.N. Sanz-Ortiz, J. Reguera, L.M. Liz-Marzán, M.C. Moreno-Bondi, Multibranched gold−-mesoporous silica nanoparticles coated with a molecularly imprinted polymer for label-free antibiotic surface-enhanced Raman scattering analysis, Chem. Mater. 28 (2016) 7947–7954.
[31] H. Wang, N.J. Halas, Mesoscopic Au "meatball" particles, Adv. Mater. 20 (2008) 820–825.
[32] S.H. Cho, H.S. Han, D.J. Jang, K. Kim, M.S. Kim, Raman spectroscopic study of 1,4-benzenedithiol adsorbed on silver, J. Phys. Chem. 99 (1995) 10594–10599.
[33] S.W. Joo, S.W. Han, K. Kim, Adsorption of 1,4-benzenedithiol on gold and silver surfaces: surface-enhanced Raman scattering study, J. Colloid Interface Sci. 270 (2001) 391–399.
[34] H. Watanabe, N. Hayazawa, Y. Inouye, S. Kawata, DFT vibrational calculations of rhodamine 6G adsorbed on silver: analysis of tip-enhanced Raman spectroscopy, J. Phys. Chem. B 109 (2005) 5012–5020.
[35] D.J. Ecobichon, Pesticide use in developing countries, Toxicology 160 (2001) 27–33.
[36] T.X. Yang, Z.Y. Zhang, B. Zhao, R.Y. Hou, A. Kinchla, J.M. Clark, L.L. He, Real-time and in situ monitoring of pesticide penetration in edible leaves by surface-enhanced Raman scattering mapping, Anal. Chem. 88 (2016) 5243–5250.

Jingxing Guo is a PhD candidate in School of Chemistry and Chemical Engineering, Nanjing University, China. His research focuses on new SERS analytical methods.

Yunlong Chen is a research associate in School of Chemistry and Chemical Engineering, Nanjing University, China. His major research focuses on methodology for cellular glycan analysis.

Jianqi Li is an ungraduated student in Nanjing University, China. His research interest is design and synthesis of new SERS substrates.

Jintong Liu is a PhD candidate in School of Chemistry and Chemical Engineering, Nanjing University, China. Her research focuses on photodynamic therapy of cancer.

Huangxian Ju received his BS, MS and PhD degrees from Nanjing University during 1982–1992. He was a postdoc in Montreal University (Canada) from 1996 to 1997 and a guest professor in three universities of Germany and Ireland in 1999–2000. He became an associate and full professor of Nanjing University in 1993 and 1999. He is currently the director of State Key Laboratory of Analytical Chemistry for Life Science. His research interests focus on analytical biochemistry, biosensing and molecular diagnosis. He has published 616 papers in different journals with h-index of 83 (Google Scholar h-index 91 with about 29,523 citations).